AD-A112 607 CALIFORNIA UNIV LOS ANGELES INTEGRATED ELECTROMAGNET--ETC F/G 9/5
ON THE EFFECT OF SUBSTRATE THICKNESS AND PERMITTIVITY ON PRINTE--ETC(U)
DEC 81 P B KATEHI, N G ALEXOPOULOS DAAG29-79-C-0050

UNCLASSIFIED UCLA-ENG-81-40 ARO-15965.10-EL NL

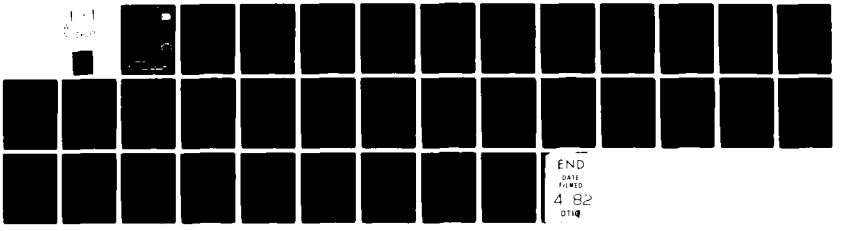

END
DATE FILMED
4 82
DTIC

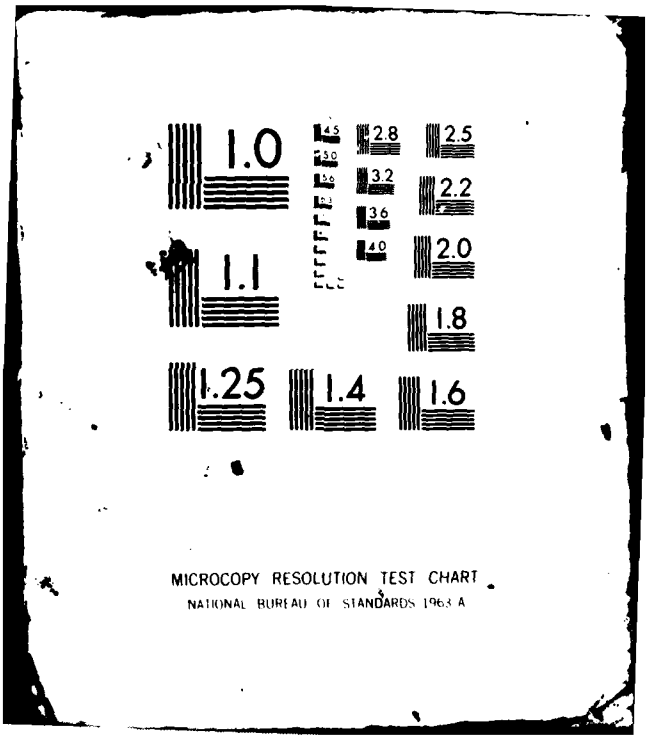
1.0
1.1
1.25
1.4
1.6
1.8
2.0
2.2
2.5
2.8
3.2
3.6
4.0
MICROCOPY RESOLUTION TEST CHART
NATIONAL BUREAU OF STANDARDS 1963 A

AD A112607

DECEMBER,

"ON THE EFFECT OF SUBSTRATE THICKNESS AND PERMITTIVITY ON PRINTED CIRCUIT DIPOLE PROPERTIES"

ELECTE
MAR 29 1982
B

by

P.B. Katehi and
N.G. Alexopoulos

Sponsored by:

U.S. Army Contract DAAG 29-79-C-0050
U.S. Navy Contract N00014-79-C-0856

SECURITY CLASSIFICATION OF THIS PAGE (When Data Entered)

REPORT DOCUMENTATION PAGE	READ INSTRUCTIONS BEFORE COMPLETING FORM
1. REPORT NUMBER	2. GOVT ACCESSION NO. AD-A112 607 / 3. RECIPIENT'S CATALOG NUMBER
4. TITLE (and Subtitle) On the Effect of Substrate Thickness and Permittivity on Printed Circuit Dipole Properties.	5. TYPE OF REPORT & PERIOD COVERED Technical Laboratory Report 6. PERFORMING ORG. REPORT NUMBER
7. AUTHOR(s) P. B. Katehi and N. G. Alexopoulos	8. CONTRACT OR GRANT NUMBER(s) DAAG 29-79-C-0050 N0014-79-C-0856
9. PERFORMING ORGANIZATION NAME AND ADDRESS Electrical Engineering Department UCLA Los Angeles, CA 90024	10. PROGRAM ELEMENT, PROJECT, TASK AREA & WORK UNIT NUMBERS
11. CONTROLLING OFFICE NAME AND ADDRESS Dr. James Mink ARO - P 4800-C-81	12. REPORT DATE December 1981 13. NUMBER OF PAGES 31
14. MONITORING AGENCY NAME & ADDRESS(if different from Controlling Office) Army Research Office Research Triangle Park North Caroline	15. SECURITY CLASS. (of this report) Unclassified 15a. DECLASSIFICATION/DOWNGRADING SCHEDULE

16. DISTRIBUTION STATEMENT (of this Report)

Reproduction in whole or in part is permitted for any purpose of the U.S. Government

DISTRIBUTION STATEMENT A
Approved for public release;
Distribution Unlimited

17. DISTRIBUTION STATEMENT (of the abstract entered in Block 20, if different from Report)

18. SUPPLEMENTARY NOTES

THE VIEW, OPINIONS, AND/OR FINDINGS CONTAINED IN THIS REPORT ARE THOSE OF THE AUTHOR(S) AND SHOULD NOT BE CONSTRUED AS AN OFFICIAL DEPARTMENT OF THE ARMY POSITION, POLICY, OR DECISION, UNLESS SO DESIGNATED BY OTHER DOCUMENTATION.

19. KEY WORDS (Continue on reverse side if necessary and identify by block number)

Substrate Permittivity
Printed Circuit Dipole
Epsilon Tube

20. ABSTRACT (Continue on reverse side if necessary and identify by block number)

The effect of substrate thickness and relative permitticity on the radiation properties of printed circuit dipoles (PCD's) is investigated. A trade-off between substrate thickness and resonant input resistance, bandwidth and radiation efficiency is presented for a PTFE glass random fiber substrate. It is found that for a fixed substrate thickness B, the resonant length and directivity decrease with increasing relative dielectric constant ε_r. The E-plane normalized power pattern is also examined as a function of ε_r and

DD FORM 1 JAN 73 1473 EDITION OF 1 NOV 65 IS OBSOLETE
S/N 0102-LF-014-6601

SECURITY CLASSIFICATION OF THIS PAGE (When Data Entered)

Classification 20. (Continued)

B. It is shown that even for very thin substrates, multiple beam radiation can result for certain values of ε_r by the excitation of surface waves. Multiple beam patterns can also be obtained with increasing B for a given ε_r. In fact, as B increases it is determined that the resonant length, bandwidth and resonant resistance approach the apparent value of a PCD on a dielectric half space.

On the Effect of Substrate Thickness and Permittivity on Printed Circuit Dipole Properties.

P. B. Katehi and N. G. Alexopoulos
Electrical Engineering Department
University of California, Los Angeles, CA 90024

This work was supported by the U.S. Army under Contract DAAG29-79-C-0050 and by the U.S. Navy under Contract N00014-79-C-0856.

Abstract

The effect of substrate thickness and relative permittivity on the radiation properties of printed circuit dipoles (PCD's) is investigated. A trade-off between substrate thickness and resonant input resistance, bandwidth and radiation efficiency is presented for a PTFE glass random fiber substrate. If is found that for a fixed substrate thickness B, the resonant length and directivity decrease with increasing relative dielectric constant ϵ_r . The $\overline{E}$-plane normalized power pattern is also examined as a function of ϵ_r and B. It is shown that even for very thin substrates, multiple beam radiation can result for certain values of ϵ_r by the excitation of surface waves. Multiple beam patterns can also be obtained with increasing B for a given ϵ_r. In fact, as B increases it is determined that the resonant length, bandwidth and resonant resistance approach the apparent value of a PCD on a dielectric half space.

Accession For	
NTIS CRA&I	☑
DTIC TAB	☐
Unannounced	☐
Justification	
PER FORM 50	
By	
Distribution/	
Availability Codes	
Dist	Avail and/or Special
A	

DTIC COPY INSPECTED 2

Introduction.

Printed circuit dipoles (PCDs) have been successfully employed in conformal arrays [1] - [3]. Recently, Elliott and Stern [4] and Stern and Elliott [5] demonstrated a design procedure for the construction of small arrays consisting of electromagnetically coupled microstrip dipoles. Implicit in their approach is the accurate knowledge of mutual coupling and array element optimization. In the aforementioned applications the dipoles were printed on very thin substrates (compared to free space wavelength). In the millimeter and submillimeter frequency range PCDs have been utilized in detector and imaging arrays with several wavelength thick substrates (see Rutledge et al. [6] - [8]). The performance characteristics of PCDs depend in a very crucial way on the substrate thickness B and substrate relative dielectric constant ϵ_r. This is due to the fact that ϵ_r and B control the amount of energy coupled into surface wave modes guided by the substrate [9] - [12]. Consequently, the radiation efficiency, (i.e., the ratio of energy radiated by the antenna into free space to that coupled in the substrate), input impedance, radiation pattern and bandwidth need to be investigated as functions of ϵ_r and B.

In this paper, a trade-off study of ϵ_r and B on the PCD properties is carried out. As a specific example of substrate thickness effect on antenna properties a PTFE glass random fiber substrate material is considered with $\epsilon_r = 2.35$. The results presented herein are based on refined analytical and numerical extentions of the information on printed dipoles contained in [9] - [11].

II. Analytical Formulation.

A precise understanding of the effect of substrate thickness and relative permittivity on the characteristics of printed circuit dipoles requires the development of integral equation solutions for the antenna current distribution. The integral equation for the PCD is given in its general form by (see figure 1)

$$\bar{E}(x,y,z) = \int_0^L \left[k_0^2 \bar{\bar{I}} + \nabla\nabla\right] \cdot \bar{\bar{G}}(\bar{r}/\bar{r}') \cdot \bar{J}(\bar{r}')dr' \qquad (1)$$

where L is the length of the dipole, $\bar{\bar{I}}$ is the unit dyadic $\bar{\bar{I}} = \hat{x}\hat{x} + \hat{y}\hat{y} + \hat{z}\hat{z}$, $\bar{J}(\bar{r}')$ is the unknown current density distribution and $\bar{\bar{G}}(\bar{r}/\bar{r}')$ is the dyadic Green's function [9] - [10] for the problem of interest. For the case of a PCD oriented along the $\hat{x}$-direction and with h = 0 [12] equation (1) simplifies to

$$E_x = \int_0^L \left[k_0^2 G_x + \frac{\partial^2}{\partial x^2}(G_x - G)\right] J_x dx' \qquad (2)$$

where [10], [12]

$$G_x = -\frac{j\omega\mu_0}{2\pi k_0^2}(1-\epsilon_r)\int_0^\infty J_0(\lambda\rho)\left(\frac{\sinh(uB)}{f_1(\lambda,B)}\right)\left(\frac{\sinh(uB)}{f_2(\lambda,B)}\right)u\lambda d\lambda \qquad (3)$$

$$G = -\frac{j\omega\mu_0}{2\pi k_0^2}(\epsilon_r-1)\int_0^\infty J_0(\lambda\rho)\left(\frac{\sinh(uB)}{f_1(\lambda,B)}\right)\left(\frac{\cosh(uB)}{f_2(\lambda,B)}\right)u_0\lambda d\lambda \qquad (4)$$

$$f_1(\lambda,B) = u_0\sinh(uB) + u\cosh(uB) \qquad (5)$$

$$f_2(\lambda,B) = \epsilon_r u_0\cosh(uB) + u\sinh(uB) \qquad (6)$$

$$\rho = \left[(x-x')^2 + (y-y')^2\right]^{1/2} \qquad (7)$$

and

$$u_o = \left[\lambda^2 - k_o^2\right]^{1/2} \quad , \quad u = \left[\lambda^2 - k^2\right]^{1/2} \tag{8}$$

The zeros of $f_1(\lambda,B)$, $f_2(\lambda,B)$ in the denominator of equations (4), (5) for $k_o < \lambda < k$ correspond to TM, TE surface wave modes [9] - [12] respectively with a TM mode having zero cut-off. The number of excited surface wave modes depends on the substrate thickness B and relative dielectric constant ε_r. By employing the method of moments [13] with a basis set of overlapping piecewise-simusoidal currents the integral equation as given by equation (2) can be discretized into a matrix form [V] = [Z] [I] where the elements of [Z] can be written as

$$Z_{ij} = \frac{1}{\left[\sin k_o l_x\right]^2} \cdot \left\{ \sum_{\nu=-1,0} \sum_{\nu'=-1,0} k_o^2 \int_{x_{i+\nu}}^{x_{i+\nu+1}} dx \int_{x_{j+\nu'}}^{x_{j+\nu'+1}} dx' \cdot \right.$$

$$\sin\left[k_o \mid l_x \nu + (x_{i+\nu+1} - x) \mid\right] \sin\left[k_o \mid l_x \nu' + (x_{j+\nu+1} - x') \mid\right] \cdot$$

$$G\left(\sqrt{(x-x')^2 + (y-y')^2}\right) + \sum_{\nu=-1,0} \sum_{\nu'=-1,0,1} k_o \left[1 - (2\cos k_o l_x + 1)\delta(\nu')\right]$$

$$\cdot \int_{x_{i+\nu}}^{x_{i+\nu+1}} \sin\left[k_o \mid l_x \nu + (x_{k+\nu+1} - x) \mid\right] \cdot \left[G_x\left(\sqrt{(x-x')^2 + (y-y')^2}\right) - \right.$$

$$\left. \left. - G\left(\sqrt{(x - x_{j+\nu'})^2 + (y-y')^2}\right)\right]\right\} \tag{9}$$

In equation (9) $l_x = L/N$ where N is the total number of subsections the dipole is divided in. By inversion the current distributions can be obtained for arbitrary parameters ε_r, B and L for center-fed thin (radius = $10^{-4}\lambda_o$) dipoles.

Computation of the matrix elements Z_{ij} involves integration of Sommerfeld type of integrals along the real λ-axis [9], [10] for which efficient routines have been written [12].

III. Effect of Substrate Permittivity Variation

The relative permittivity is varied for a fixed substrate thickness of $B = 0.1016\lambda_0$. For values of ϵ_r up to $\epsilon_r = 45$ and for the chosen B there are three surface wave modes that can be excited. The antenna resonant length L_r is shown in figure 2 as a function of ϵ_r. As more energy is coupled into guided waves inside the substrate the resonant length decreases with a cusp discontinuity exhibited at every value of ϵ_r where the onset of the next surface wave mode occurs. Figure 2 implies that the radiation efficiency of the PCD decreases with increasing ϵ_r. The dependence of the input impedance Z_{in} on ϵ_r is demonstrated in figures 3 - 5, where Z_{in} is plotted vs. antenna length L for $\epsilon_r = 2, 10, 35$ respectively and for $B = 0.1016\lambda_0$. As ϵ_r increases the following effects can be observed: (a) The value of the total input resistance R decreases. (b) The reactance becomes increasingly capacitive with a reduced number of resonances.

IV. Substrate Thickness Variation.

A PTFE glass random fiber substrate is selected with $\epsilon_r = 2.35$ to analyze the effect of increasing B. The variation of PCD resonant length vs. B is demonstrated in figure 6 wherefrom it is concluded that as $B \rightarrow \infty$, $L_r \rightarrow 0.375\lambda_0$ which is anticipated to be the resonant length of a wire dipole of radius

$a = 10^{-4}\lambda_0$ on a dielectric half-space with $\epsilon_r = 2.35$. Figure 7 demonstrates the dependence of PCD resonant resistance on B. It is worth mentioning that for $B = 1.2\lambda_0$ there exist 6 excited modes in the substrate. As $B \rightarrow \infty$, $R_r \rightarrow 50$ ohms. Figure 8 shows the radiation efficiency $\eta = \frac{R_{rr}}{R_{rs}}$ where $R_r = R_{rr} + R_{rs}$, R_{rr} being the radiation resonant resistance and R_{rs} the surface wave resonant resistance respectively. The bandwidth of the PCD is exhibited in figure 9 vs. B. The bandwidth has been defined here as

$$BW = \frac{1}{L_r}\left[\frac{2R_r}{\frac{dX}{d(L/\lambda)}\Big|_{L_r}}\right] \qquad [10]$$

These curves provide a trade-off analysis for a PCD as e.g. if we wish to choose a maximum radiation efficiency dipole with $\eta \equiv 4$ at $B = 0.2\lambda_0$, then the resonant length is $L_r = 0.369345\lambda_0$, $R_r = 90$ ohms and BW = 18%. The corresponding $\bar{E}$-plane normalized radiation pattern is shown in figure 10, where it is observed that the half-power beamwidth is approximately 70 degrees. On the other hand if an input $R_r = 50$ ohms is desired then $B \equiv 0.12\lambda_0$, BW = 8% and $\eta \equiv 2.8$.

V. Radiation Pattern

It is of interest to investigate now the dependence of the far-field pattern on substrate properties. The far-zone electromagnetic field can be obtained by a saddle-point method and the electric field components are given by

$$E_\theta = 2k_0^2 \Pi_\theta \tag{11}$$

and

$$E_\phi = 2k_0^2 \Pi_\phi \tag{12}$$

where

$$\Pi_\theta = -j100 \frac{e^{-jk_0R}}{R} \cos\phi \cdot \left(\frac{\cos[k_0 \ell_x \sin\theta\cos\phi] - \cos(k_0\ell_x)}{k_0 \sin(k_0\ell_x[1 - \sin^2\theta\cos^2\phi])} \right)$$

$$\cdot \left[\cos\theta \, \phi(\varepsilon_r, B, \theta) + (\varepsilon_r - 1)\sin\theta\Psi(\varepsilon_r, B, \theta) \right] \sum_{n=1}^{N} I_n e^{jnk_0\ell_x\sin\theta\cos\phi}, \tag{13}$$

$$\Pi_\phi = j100 \frac{e^{-jk_0R}}{R} \sin\phi \cdot \left(\frac{\cos[k_0 \ell_x \sin\theta\cos\phi] - \cos(k_0\ell_x)}{k_0 \sin(k_0\ell_x[1 - \sin^2\theta\cos^2\phi])} \right) \cdot$$

$$\phi(\varepsilon_r, B, \theta) \sum_{n=1}^{N} I_n e^{jnk_0\ell_x\sin\theta\cos\phi}, \tag{14}$$

$$\phi(\varepsilon_r, B, \theta) = \frac{1}{k_0} \left\{ \frac{1}{1 - j \dfrac{\sqrt{\varepsilon_r - \sin\theta}}{\cos\theta} \cot(k_0\sqrt{\varepsilon_r - \sin^2\theta})} \right\} \tag{15}$$

and

$$\Psi(\varepsilon_r,B,\theta) = \frac{\tan\theta}{k_0}\left(\frac{1}{1 - j\dfrac{\sqrt{\varepsilon_r - \sin^2\theta}}{\cos\theta}\cot(k_0\sqrt{\varepsilon_r - \sin^2\theta}\ B)}\right)$$

$$\cdot\left(\frac{1}{\varepsilon_r + j\dfrac{\sqrt{\varepsilon_r - \sin^2\theta}}{\cos\theta}\tan(k_0\sqrt{\varepsilon_r - \sin^2\theta}\ B)}\right) \tag{16}$$

or

$$\Psi(\varepsilon_r,B,\theta) = \tan\theta\,\Phi(\varepsilon_r,B,\theta)\,\Lambda(\varepsilon_r,B,\theta) \tag{17}$$

with

$$\Lambda(\varepsilon_r,B,\theta) = \frac{1}{\varepsilon_r + j\dfrac{\sqrt{\varepsilon_r - \sin^2\theta}}{\cos\theta}\tan(k_0\sqrt{\varepsilon_r - \sin^2\theta}\ B)} \tag{18}$$

An investigation of the expressions given for the far-zone electric field indicates that the effect of the substrate properties on the radiation pattern is controlled by the factors $\Phi(\varepsilon_r,B,\theta)$ and $\Lambda(\varepsilon_r,B,\theta)$. Furthermore, it is verified that $\Phi(\varepsilon_r,B,\theta)$ is a result of the substrate guided TM modes, while $\Lambda(\varepsilon_r,B,\theta)$ is due to the TE modes. A thorough analysis of Φ and Λ indicates that Φ determines the position of nulls, principal as well as secondary maxima of the pattern for $\theta < \pi/2$. On the other hand the factor Λ affects the sidelobe maxima only and in general it smooths out the pattern. In summary, the following results can be stated for the dependence of the radiation pattern on ε_r and B.

A. Fixed Substrate Thickness.

For fixed substrate thickness B and varying relative dielectric constant ϵ_r we find:

1. If $1 + (\frac{n}{2})^2 (\frac{\lambda_o}{B})^2 \leq \epsilon_r < (\frac{n+1}{2})^2 (\frac{\lambda_o}{B})^2$, integer n (19)

the radiation pattern consists of one lobe only.

2. If $(\frac{n}{2})^2 (\frac{\lambda_o}{B})^2 \leq \epsilon_r < 1 + (\frac{n}{2})^2 (\frac{\lambda_o}{B})^2$, integer n (20)

there may exist more than one beam. Specifically if

$$[\![2\sqrt{\epsilon_r}\,\frac{B}{\lambda_o}]\!] = [\![2\sqrt{\epsilon_r - 1}\,\frac{B}{\lambda_o}]\!] + N \tag{21}$$

and

$$2\sqrt{\epsilon_r}\,\frac{B}{\lambda_o} = [\![2\sqrt{\epsilon_r - 1}\,\frac{B}{\lambda_o}]\!] + N + a \tag{22}$$

where $[\![\ ]\!]$ indicates integer value of, N is an integer and a an arbitrary real positive number then

i) If N = 0 (a > 0), there exists a single lobe only.

ii) If N > 0, a > 0, there exist 2N + 1 lobes with one of the maxima always at $\theta = 0$.

iii) If N > 0, a = 0, there exist 2N lobes, with a null at $\theta = 0$.

B. Fixed Substrate Permittivity.

In this case the following conclusions can be drawn:

1. If $(\frac{n}{2})\,\frac{1}{\sqrt{\epsilon_r - 1}} \leq \frac{B}{\lambda_o} < (\frac{n+1}{2})\,\frac{1}{\sqrt{\epsilon_r}}$ (23)

with n an integer there is always one lobe at most.

2. If $(\frac{n}{2})\ \frac{1}{\sqrt{\varepsilon_r}} < \frac{B}{\lambda_0} < \frac{n}{2}\ \frac{1}{\sqrt{\varepsilon_r - 1}}$, (24)

n an integer, there may exist more than one lobes.

Again relations (21) and (22) hold. The pattern nulls as determined by $\Phi(\varepsilon_r, B, \theta)$ occur at

$$\theta_n = \pm \sin^{-1} \left[\varepsilon_r - (\frac{n\lambda_0}{2B})^2\right]^{1/2} \quad (25)$$

n an integer.

The dependence of the $\overline{E}$-plane normalized radiation power pattern on ε_r and B is now investigated. We consider again the PTFE substrate with $\varepsilon_r = 2.35$. For the optimum radiation efficiency of figure 8 the substrate thickness is $B = 0.2\lambda_0$. In this case equation (22) is satisfied for $N = 0$ and $a = 0.613$ i.e. the radiation pattern consists of a single lobe as shown in figure 10. In light of equations (21) and (22) it can be verified that for $B = 0.2\lambda_0$, $0.975\lambda_0$ and $1.05\lambda_0$ the $\overline{E}$-plane normalized power pattern will have respectively one, two and three lobes as shown in figures 11 - 13.

If the substrate thickness B is fixed, e.g. at $B = 0.1016\lambda_0$ then the $\overline{E}$-plane normalized power pattern is shown in figures 14 - 16 for $\varepsilon_r = 2,10,35$ respectively. With increasing ε_r we observe that the PCD directivity is decreased because more energy is radiated close to the $\theta = \pi/2$ direction along the length of the antenna as the number of modes guided in ths substrate increases. It is further observed in figure 17, that when $\varepsilon_r = 25$ and for $B = 0.1016\lambda_0$ there exist three lobes and according to equation (25) the nulls are at $\theta = \pm 62.111^0$. This last case is of special interest since for the given ε_r and B values there

exist three guided modes in the substrate. The zero of $f_1(u,B)$ pertaining to the dominant TM mode can be shown to occur near the branch point k_0. This explains the nature of the pattern near $\theta = \pi/2$, i.e. a strong surface wave mode is launched along the ends of the dipole and it propagates as a cylindrical wave on the substrate interface [14].

Conclusions.

It has been demonstrated in this paper that it is possible to make a precise trade-off analysis for the design of optimum printed circuit dipole elements. This has been achieved by determining the dependence of the antenna element properties on substrate thickness and relative dielectric constant. For a substrate chosen with $\varepsilon_r = 2.35$, an optimum design for a center fed dipole has been determined to require a substrate thickness of $0.2\lambda_0$. This yields an optimum radiation efficiency $\eta = 4$, i.e. the power radiated in free space is four times that which is coupled in guided modes in the substrate. This design also gives an optimum bandwidth of 18% and an input resonant resistance of 90 ohms for a resonant length of $L_r = 0.369345\lambda_0$.

References

[1] H.G. Oltman, "Electromagnetically coupled microstrip dipole antenna elements," presented at the Proc. 8th European Microwave Conference, Paris, France, Sept. 1978.

[2] D.A. Huebner, "An electrically small microstrip dipole planar array," presesnted at the Proc. Workshop on Printed Circuit Antenna Technology, New Mexico State Univ., Las Cruces, N.M. Oct. 1979.

[3] H.G. Oltman and D.A. Huebner, "Electromagnetically coupled microstrip dipoles" IEEE Trans. Antennas Propagat., vol. AP-29, pp. 151-157, Jan., 1981.

[4] R.S. Elliott and G.J. Stern, "The design of microstrip dipole arrays including mutual coupling, part I: Theory," IEEE Trans. Antennas Propagat., vol. AP-29, pp. 757-760, Sept., 1981.

[5] G.J. Stern and R.S. Elliott, "The design of microstrip dipole arrays including mutual coupling, part II: Experiment," IEEE Trans. Antennas Propagat., vol. AP-29, pp. 761-765, Sept., 1981.

[6] D.B. Rutledge, S.E. Schwartz and A.T. Adams, "Infrared and submillimeter antennas," Infrared Phys., vol. 18, pp. 713-729, 1978.

[7] T.L. Hwang, D.B. Rutledge and S.E. Schwartz, "Planar sandwitch antennas for submillimeter applications," Appl. Phys. Lett., vol. 34, pp. 9-11, 1979.

[8] D.B. Rutledge, S.E. Schwartz, T.L. Hwang, D.J. Angelakos, K.K. Mei, and S. Yokota, "Antennas and Waveguides for Far-Infrared Integrated Circuits" IEEE J. Quantum Electron., vol. QE-16, pp. 508-516, May 1980.

[9] N.K. Uzunoglu, N.G. Alexopoulos and J.G. Fikioris, "Radiation properties of microstrip dipoles," IEEE Trans. Antennas Propagat., vol. AP-27, pp. 853-858, Nov. 1979.

[10] I.E. Rana and N.G. Alexopoulos, "Current distribution and input impedance of printed dipoles," IEEE Trans. Antennas Propagat., vol. AP-29, pp. 99-105, Jan. 1981.

[11] N.G. Alexopoulos and I.E. Rana, "Mutual impedance computation between printed dipoles," IEEE Trans. Antennas Propagat. vol. AP-29, pp. 106-111, Jan. 1981.

[12] P.B. Katehi, "Printed circuit dipole characteristics for microwave, millimeter wave and submillimeter wave applications," UCLA Master's Thesis, 1981.

[13] R.F. Harrington, Field Computation by Moment Methods Macmillan, New York, 1968.

[14] P.B. Katehi and N.G. Alexopoulos, "On the nature of the electromagnetic field radiated by a printed antenna on a grounded substrate" UCLA Integrated Electromagnetics Laboratory Report No. 3, 1981.

Acknowledgements:

The authors wish to thank Professor H.J. Orchard for helpfull discussions on bandwidth definitions.

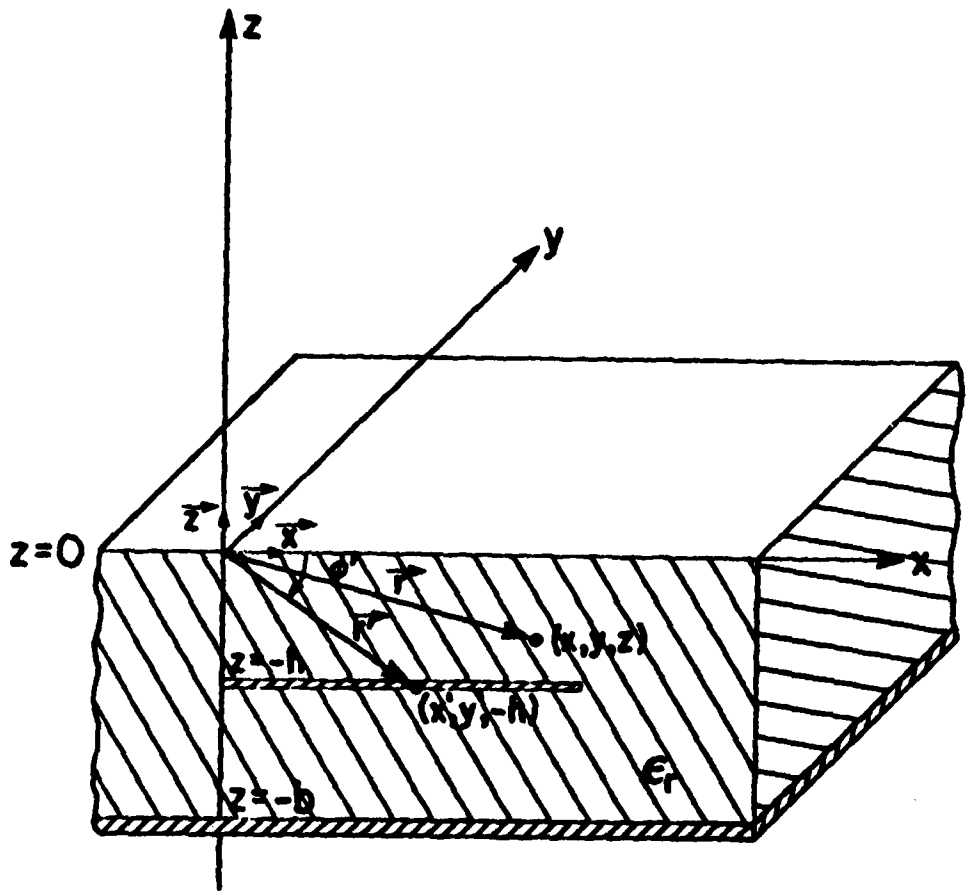

$$\vec{r}_x = \frac{\vec{r}\cos\phi'}{|\vec{r}\cos\phi'|}$$

Figure 1 : Wire Dipole Embedded in a Grounded Dielectric Slab

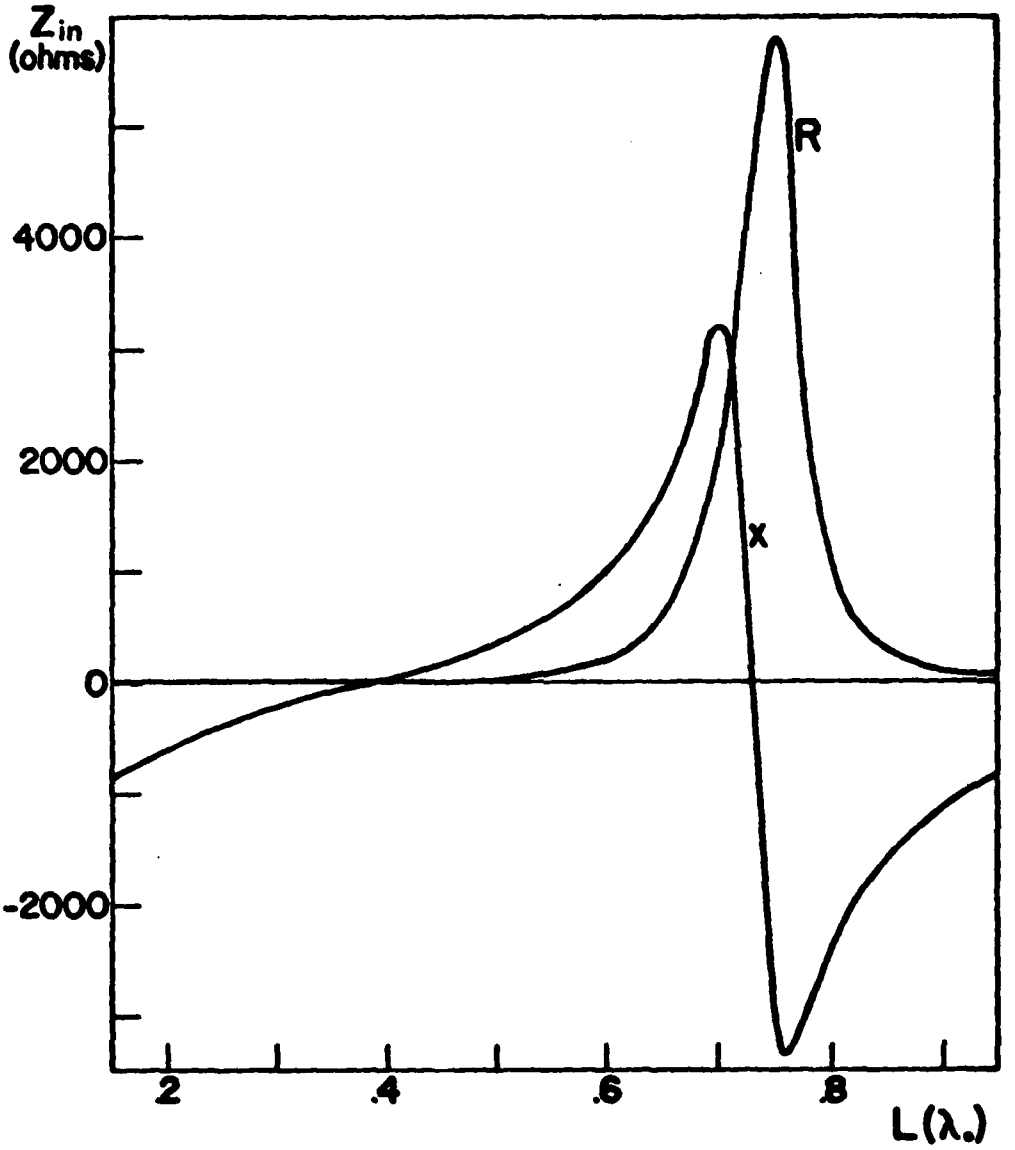

Figure 2 : Input Impedance for a Printed Dipole with $\epsilon_r=2$ and $b=0.1016\lambda_o$ Resonant Length $L_r=0.38\lambda_o$

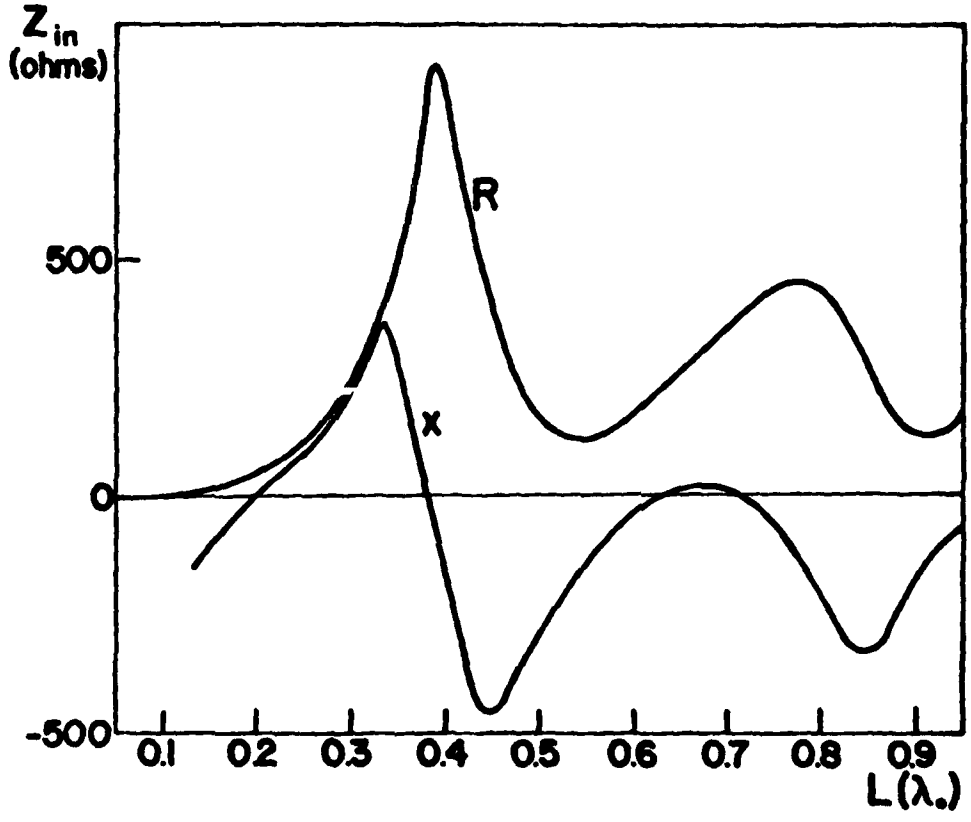

Figure 3 : Input Impedance for a Printed Dipole with $\epsilon_r=10$ and $b=0.1016\lambda_o$ Resonant Length $L_r=0.205\lambda_o$

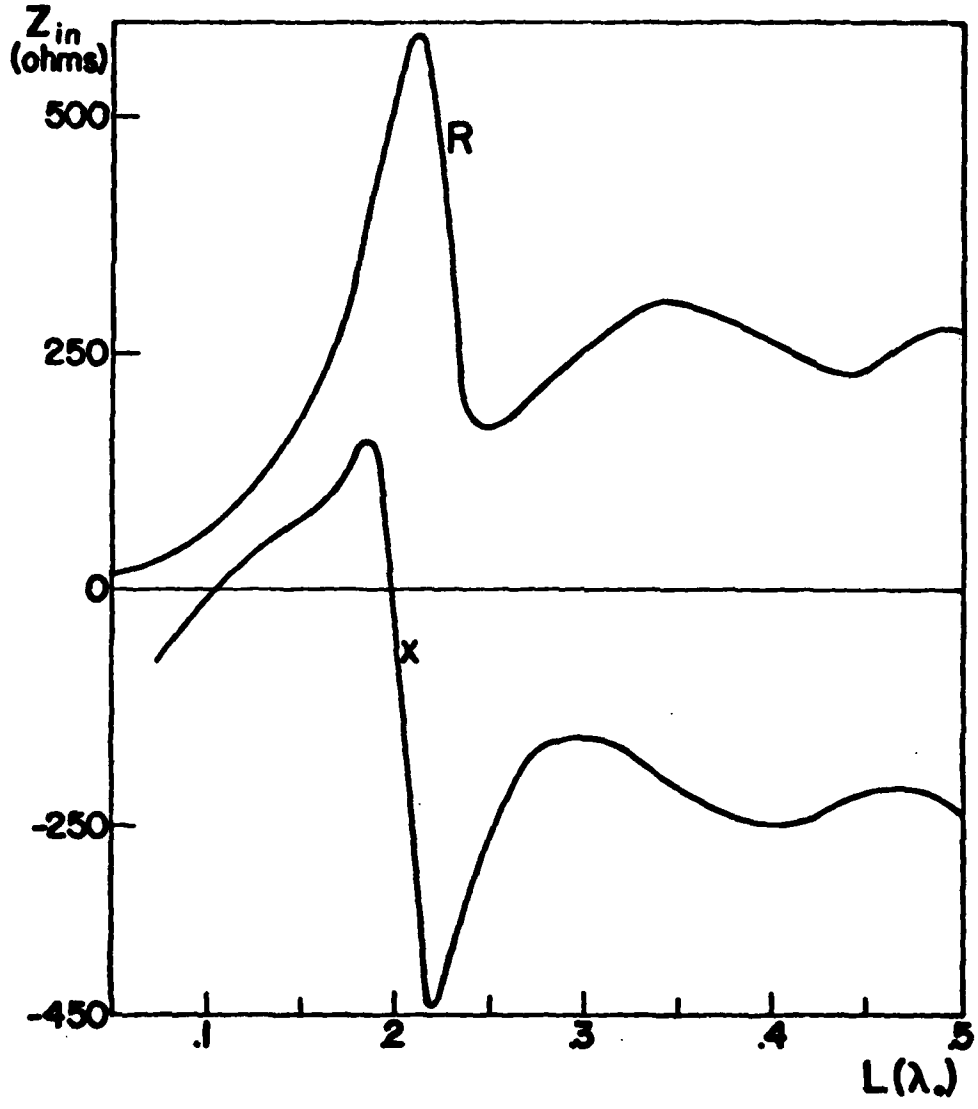

Figure 4 .: Input Impedance for a Printed Dipole with $\epsilon_r = 35$ and $b = 0.1016\lambda_o$ Resonant Length $L_r = 0.1025\lambda_o$

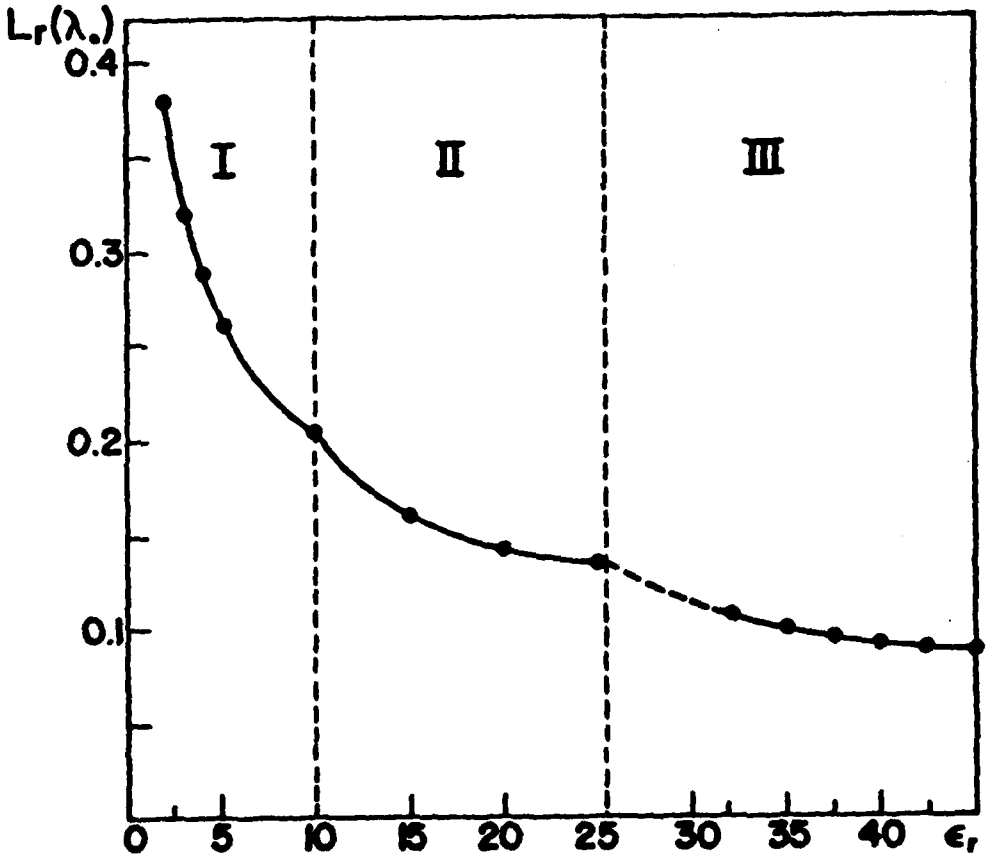

Figure 5 : Resonant Length vs. Relative Dielectric Constant ϵ_r for the Printed Dipole with $b=0.1016\lambda_o$

I: One Surface Wave

II: Two Surface Waves

III: Three Surface Waves

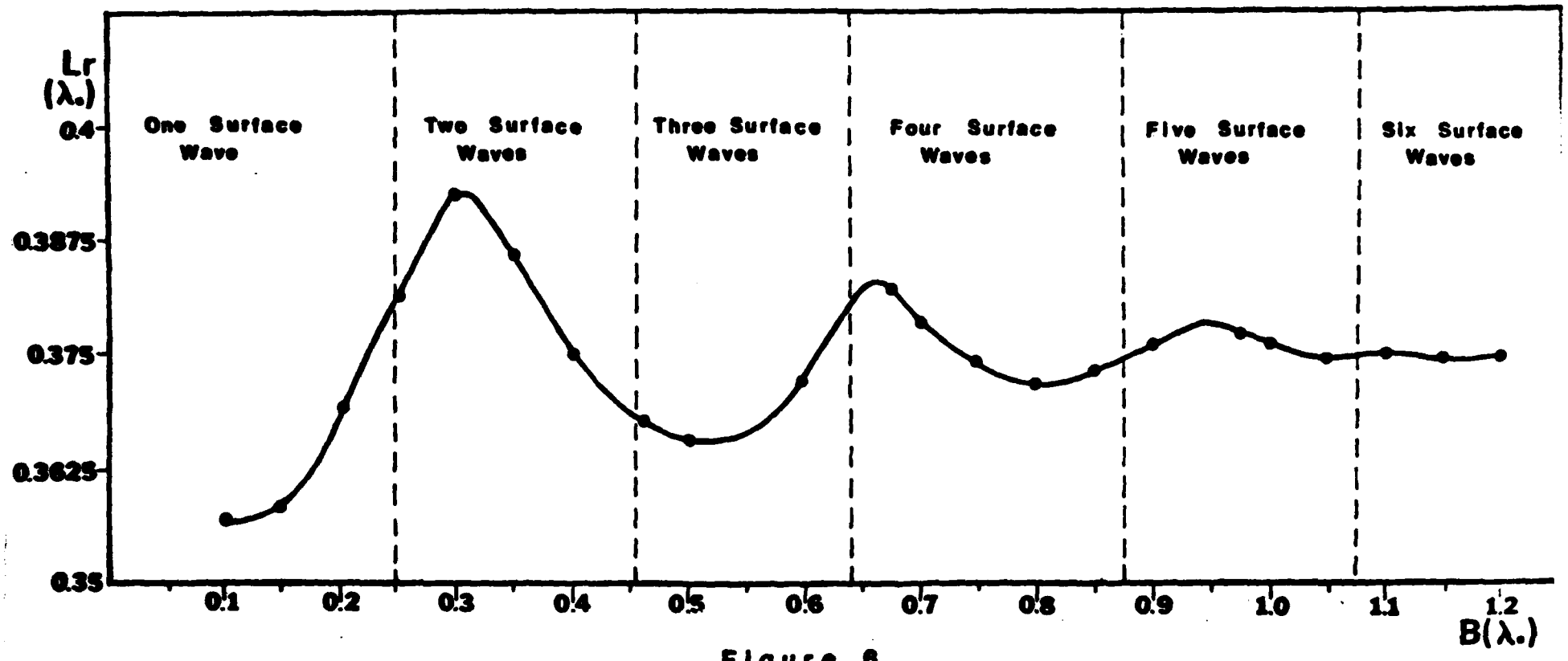

Figure 6

Resonant Length L vs. Substrate Thickness B

($\epsilon_r = 2.35$)

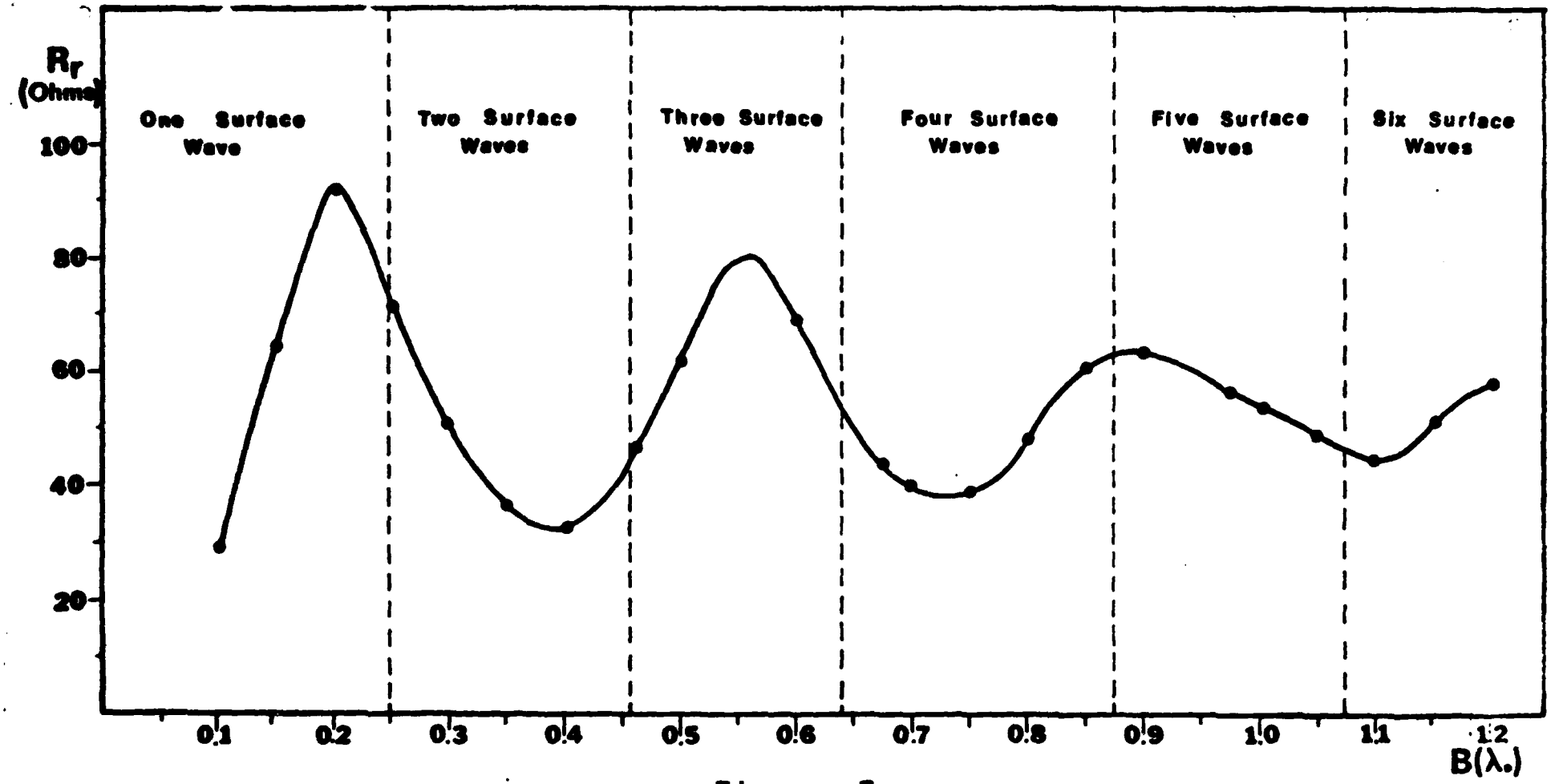

Figure 7

Resonant Resistance vs. Substrate Thickness B

($\epsilon_r = 2.35$)

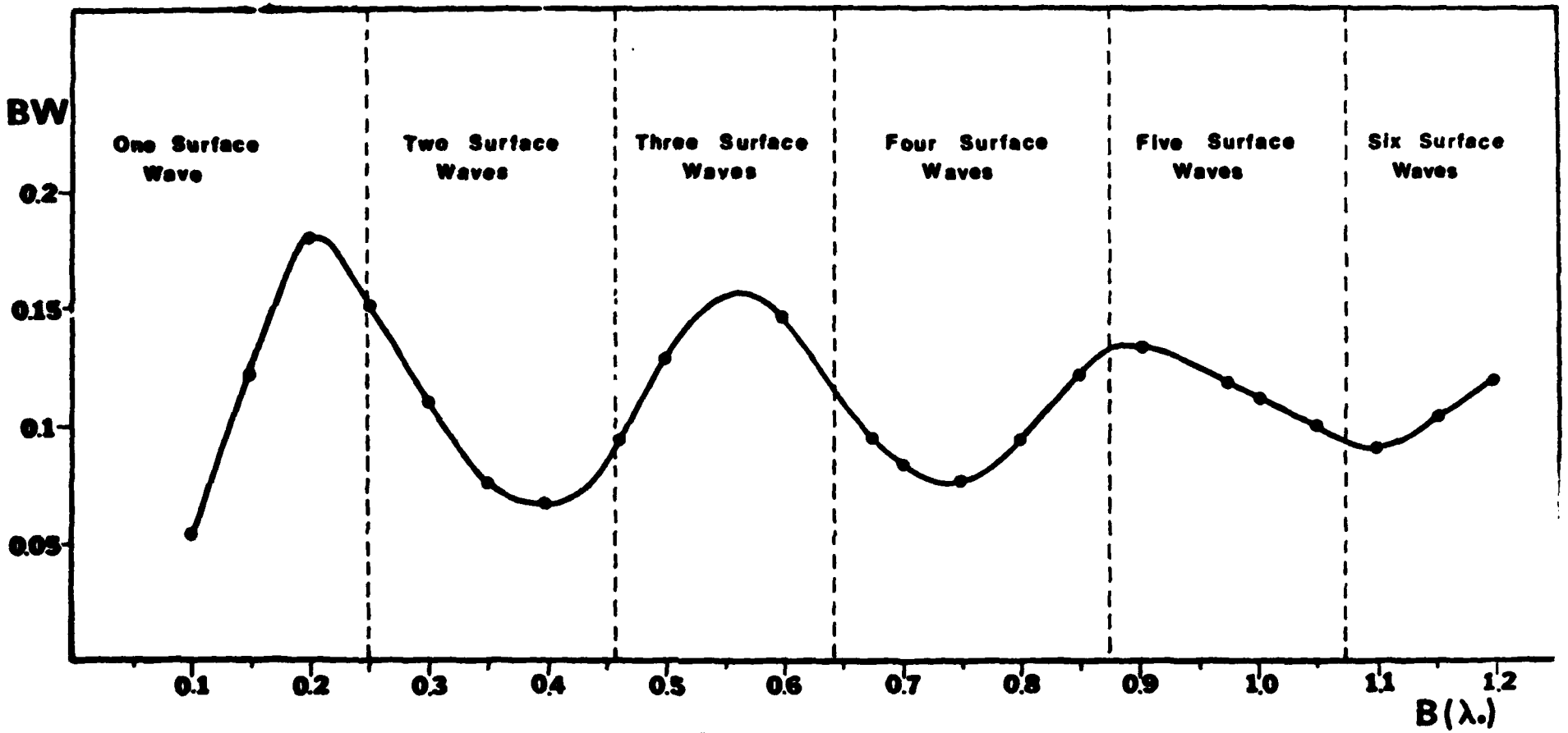

Figure 8

Bandwidth BW vs. Substrate Thickness B

(ϵ_r =2.35)

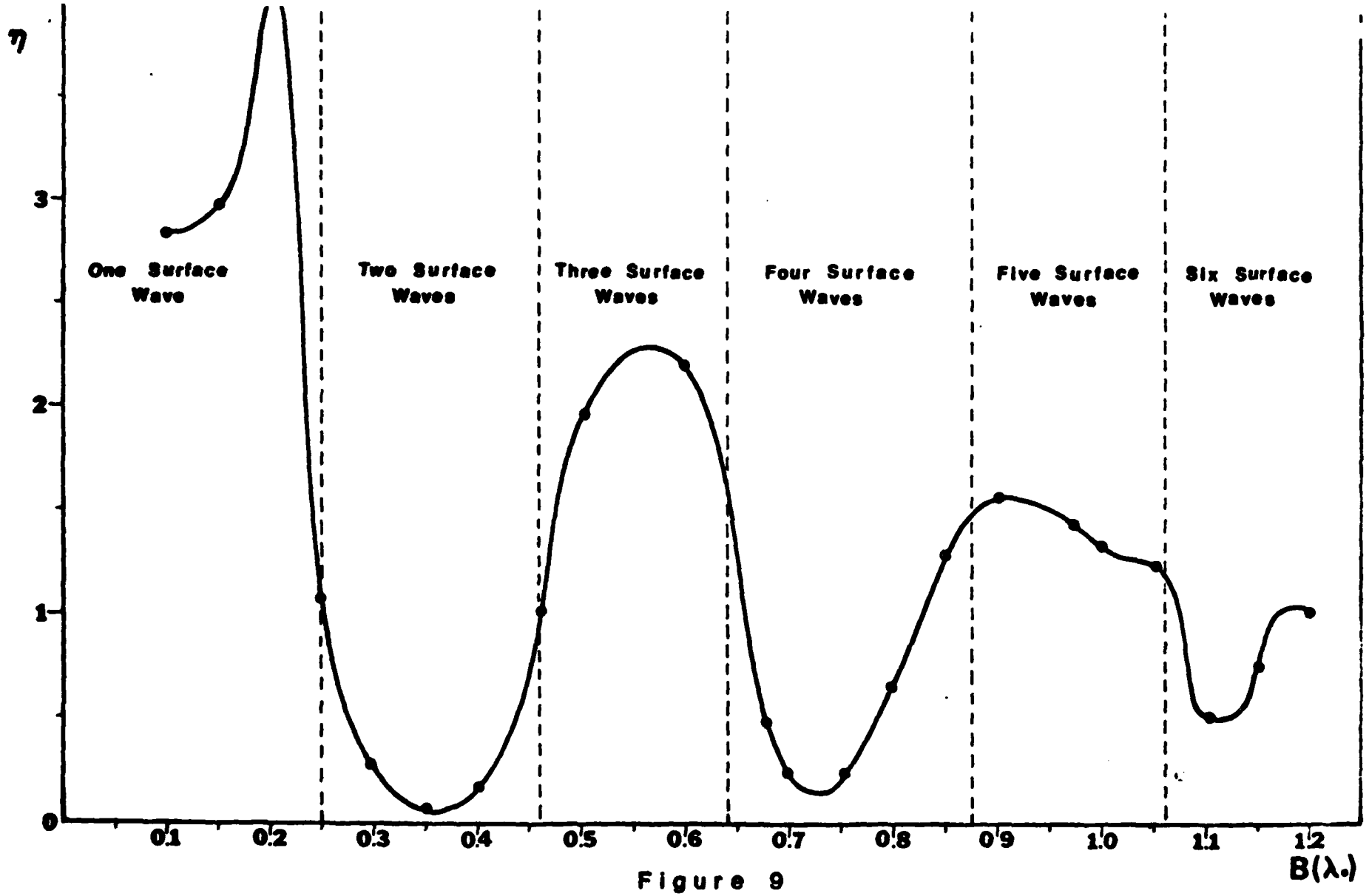

Figure 9

Efficiency η vs. Substrate Thickness B ($\epsilon_r = 2.35$)

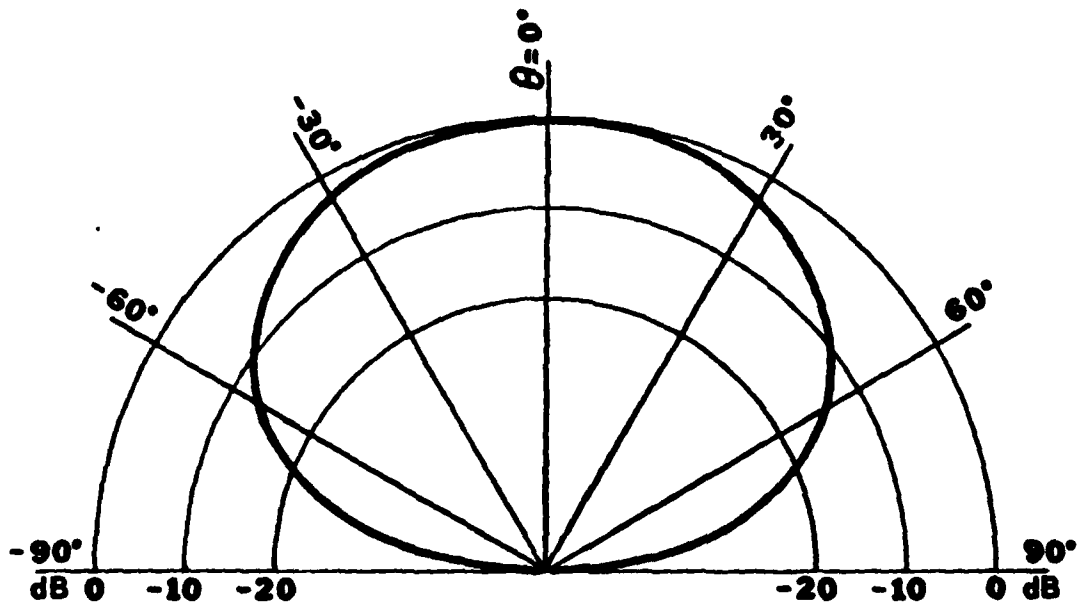

Figure 10

E-Plane Normalized Power Pattern

(ϵ_r=2.35, B=0.20λ_o, L=0.369345λ_o)

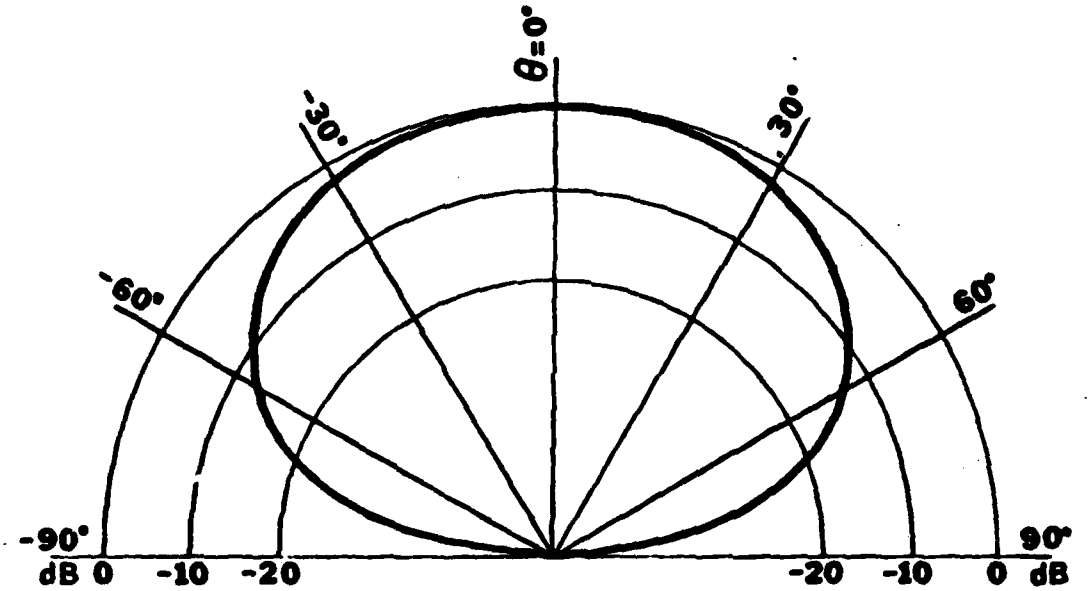

Figure 11

E-Plane Normalized Power Pattern

(ϵ_r=2.35, B=0.2λ_o, L=0.3λ_o)

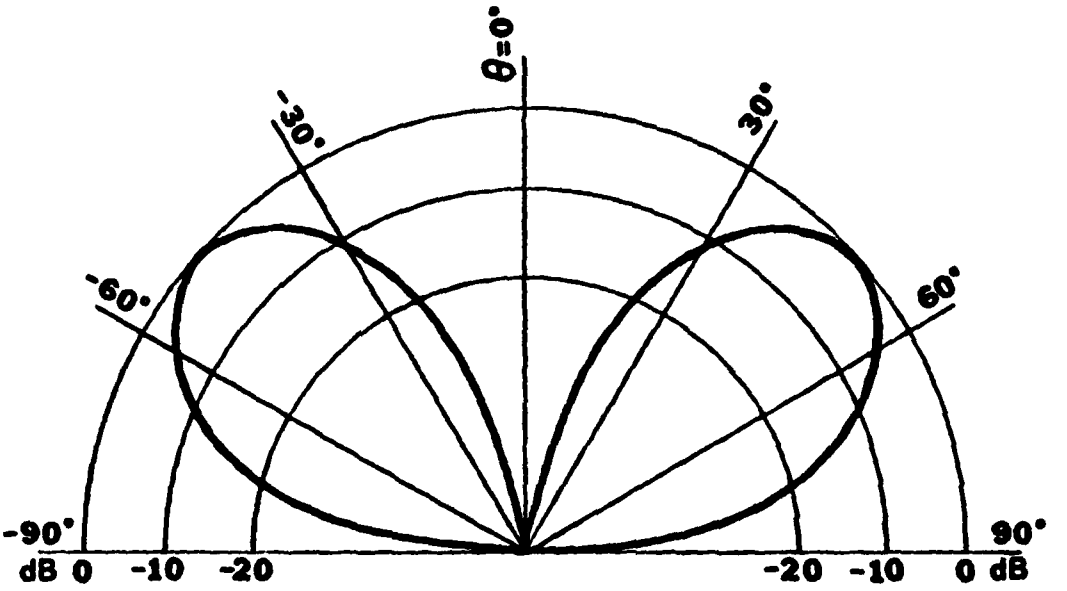

Figure 12

E-Plane Normalized Power Pattern

($\epsilon_r = 2.35, B = 0.975\lambda_o, L = 0.3\lambda_o$)

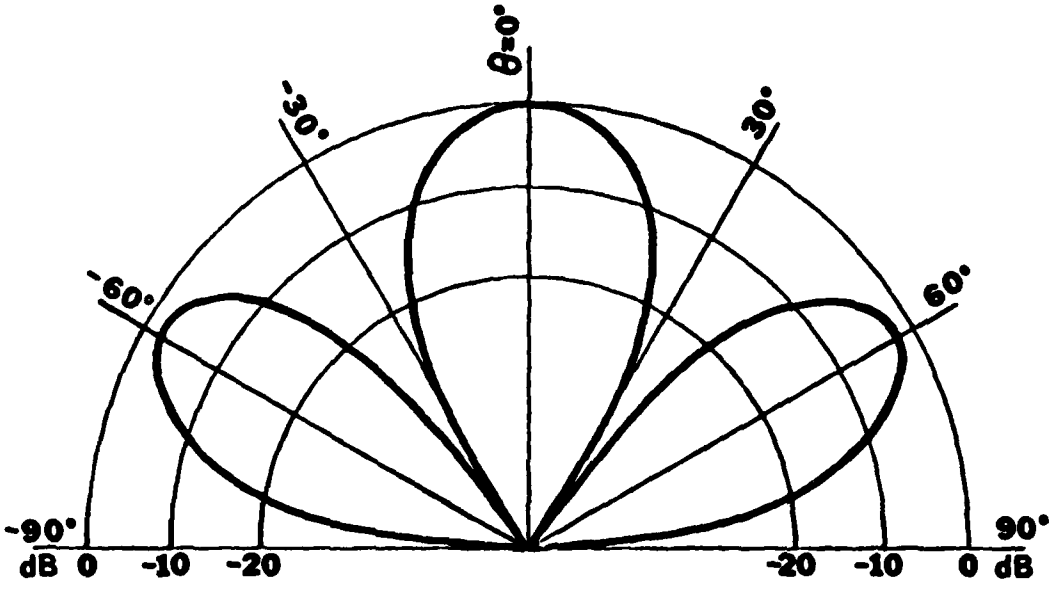

Figure 13

E-Plane Normalized Power Pattern

($\epsilon_r = 2.35, B = 1.05\lambda_o, L = 0.3\lambda_o$)

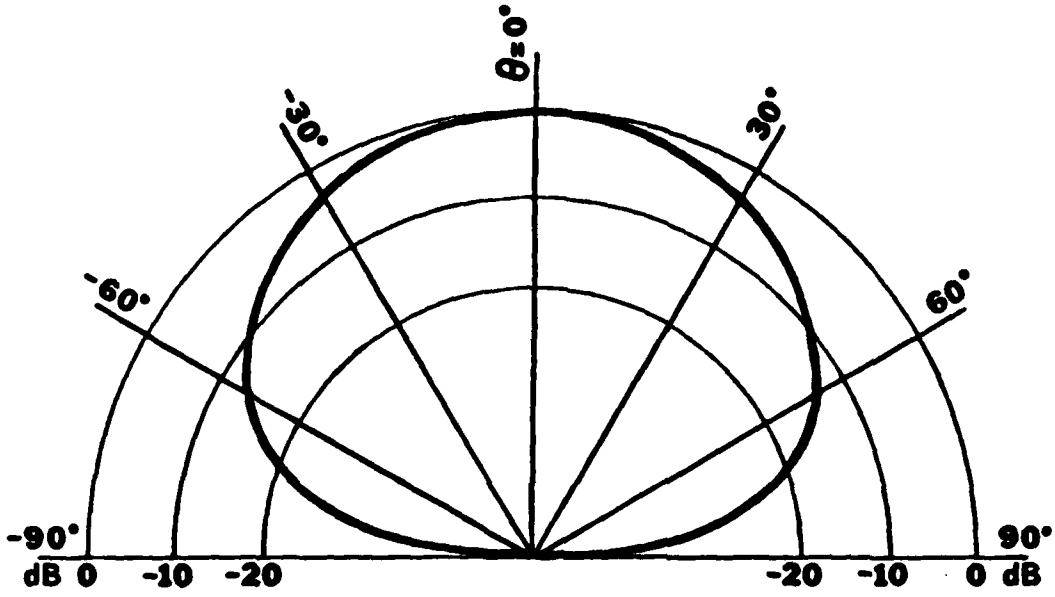

Figure 14

E-Plane Normalized Power Pattern

(ϵ_r=2.35, B=0.1016λ_o, L=0.3λ_o)

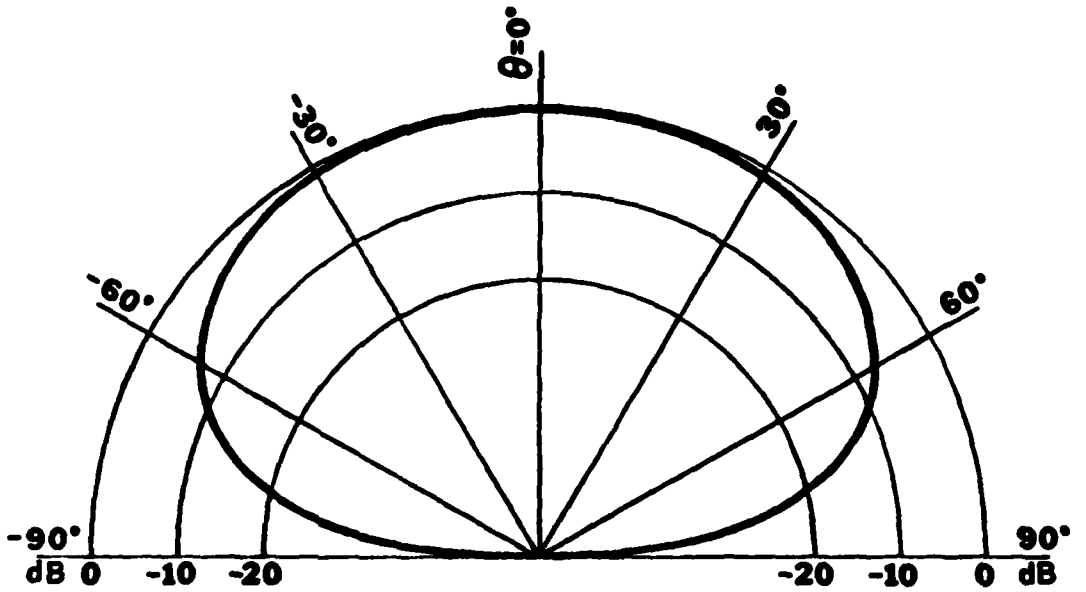

Figure 15

E-Plane Normalized Power Pattern

(ϵ_r=10.0, B=0.1016λ_o, L=0.3λ_o)

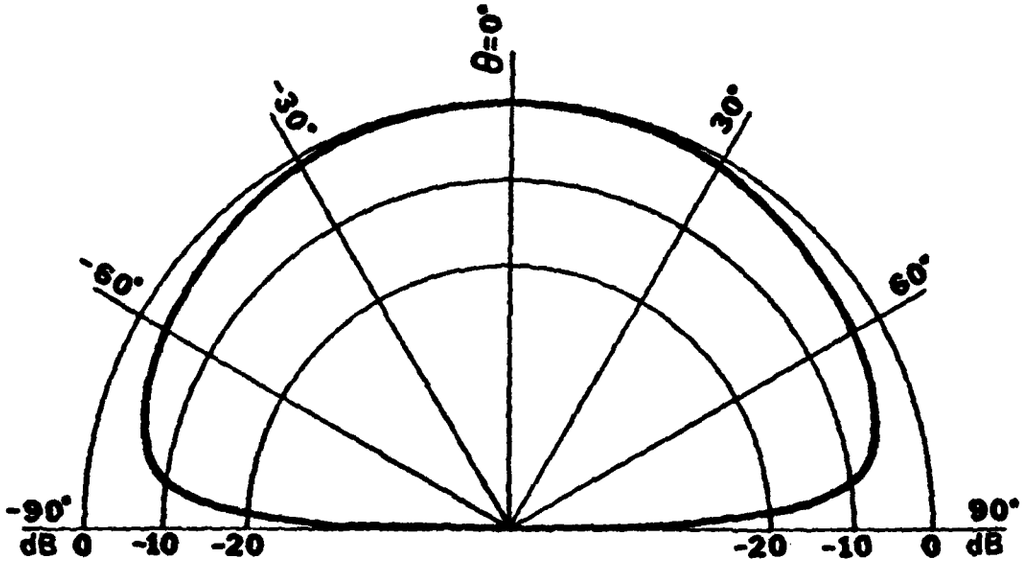

Figure 16

E-Plane Normalized Power Pattern

(ϵ_r=35.0, B=0.1016λ_o , L=0.3λ_o)

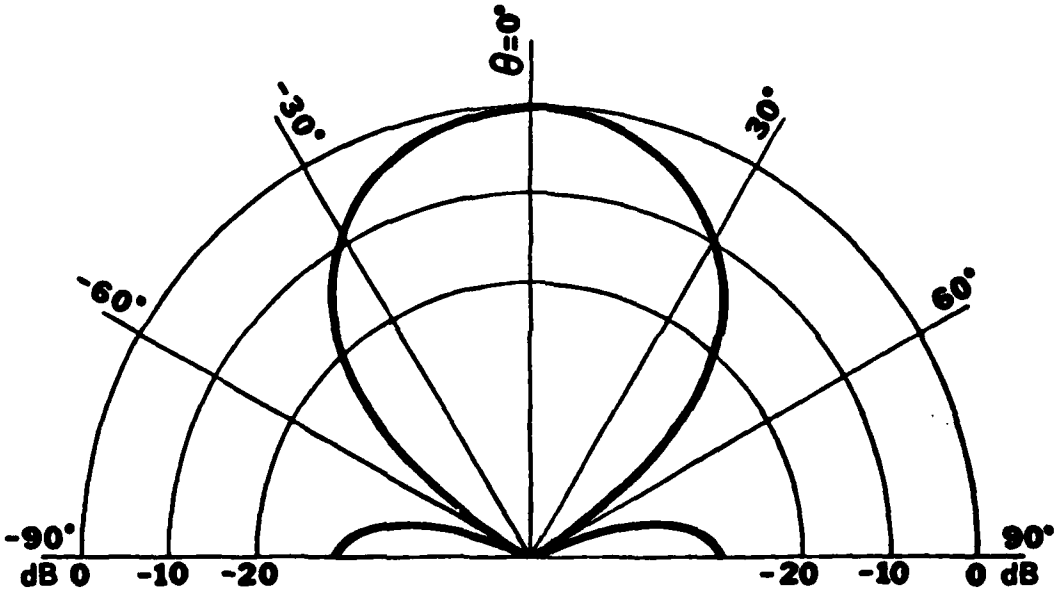

Figure 17

E-Plane Normalized Power Pattern

($\epsilon_r = 25, B = 0.1016\lambda_o, L = 0.3\lambda_o$)